Cyclic Axial Performance and Energy Dissipation of Cold-Formed Steel Zee Sections

Hanan H. Eltobgy, Anwar Badawy, Emad Darwish, Andrew Nabil

Abstract— This research investigated the axial performance of Cold-Formed Steel, CFS thin-walled Zee-shaped sections under cyclic pure axial loading. The experimental studied a zee section with a depth of 200mm and a thickness of 2mm. The experiment program was conducted for three full-scale specimens to examine the three buckling failure modes: local buckling, distortion buckling, and global buckling modes with a length of 600mm,1000 mm, and 2500 mm. The Zee-section web is provided with a notch in the distortion and global buckling specimens to prevent the local buckling formation in the web. The energy dissipation with strength degradation behavior of the Zee section was examined for the three buckling failure modes. The cyclic load-displacement protocol was performed according to the FEMA 461 method depending on the elastic properties of the CFS section. The results showed the failure mode of the CFS zee elements and investigated the axial load-displacement responses and axial load capacity. A Finite Element Model FEM was conducted and validated by the experimental results. The FEM analysis was extended to study the behavior of the cyclic Zee sections with wide ranges of Zee-sections' geometry including the lip depth, flange width, and thickness.

Index Terms— Cold-formed Steel, Zee Section, Energy Dissipation, Cyclic loading, Local buckling, Distortion buckling, Global buckling

1 INTRODUCTION

In recent years, Cold-formed steel (CFS) thin-walled sections had been become increasingly popular due to its their advantages of lightweight and high strength with less effort to form different section shapes and had widely used in current building systems. CFS sections are used in current analysis and design as part of lateral load-resisting systems as steel shear walls. These individual CFS sections are studied in form of shear wall tests to understand the seismic behavior of cold-formed steel structures, including experimental and analytical models [1-4]. CFS members sustaining compressive loads are subjected to inelastic buckling deformation that affects their strength and stiffness. In addition, when subjected to cyclic loading with reverse buckling deformation forming energy dissipation through inelastic strain accompanied by fracture or tearing in material highly stressed location [5, 6]. Evaluation methods of energy dissipation and strength degradation of thin-walled CFS are minor in standards and codes. CFS sections have been ignored in resisting the lateral loads [7-9] and are neglected in used as a lateral resisting system [10]. Padilla-Llano et al [11, 12] presented a computationally efficient CFS elements component-based experimental and analytical analysis supported by nonlinear hysterical models of for CFS members using a loading protocol adapted from FEMA 461 [13], they used ABAQUS nonlinear finite element soft package to investigate the impacts of slenderness, imperfection, and boundary conditions on the cyclic response and energy dissipation of such elements. The CFS sections were investigated under cyclic and repeated load protocols to study the performance of light-weight shear wall panels [14, 15], and portal frame elements [16-19]. To understand the performance of thin-walled elements, it is necessary to characterize the cyclic behavior for isolated CFS sections, including the three primary buckling modes (local, distortion, and global), and the capability to dissipate energy. Most of the previous research studied the performance of CFS lipped channel and box sections, and rarely studied the Zee sections, Therefore, this research aims to understand the behavior of the CFS Zee section under pure axial cyclic loading. As known, the CFS response subjected to cyclic tension loads has remained constant strength with inelastic elongation behavior. The sequence of loading direction of compression then tensions or vice versa does not affect the total energy dissipated. Jain, Hanson, et al. [6] recommended starting with a tension loading cycle to decrease the initial imperfection. CFS elements subjected to cyclic loads are significantly affected by starting local damage and rapidly losing their strength [20]. The capability of CFS sections to dissipate energy in the form of total inelastic deformation increased as the slenderness of elements decrease and is mainly affected by imperfection and residual stress [6]. The Direct Strength Method (DSM) [21] can be used to investigate the member strength and section capacity, also, to identify the three buckling failure modes: a) local buckling, b) distortion buckling, and c) global buckling. Depending on the three buckling modes, which are limit states govern, the experimental program was conducted for three full-scale cyclic tests representing the three buckling modes. In addition, more analytical parametric studies were performed to investigate the impact of the section geometry, flange width, lip depth, and thickness.

- *Associate Professor of Structural Engineering, Civil Engineering Department Faculty of Engineering at Shoubra Benha University, Email: hanan.altobgy@feng.bu.edu.eg*
- *Professor of Steel Structures and Bridges, Civil Engineering Department, Faculty of Engineering at Shoubra, Benha University, Email: Anwar.Badawy@feng.bu.edu.eg*
- *Lecturer of Structure Engineering, Civil Eng. Department, Faculty of Engineering, Shoubra, Benha University, Cairo, Egypt, Email: emad.darwish@feng.bu.edu.eg*
- *Assistant Lecturer of Structure Engineering, Civil Eng. Department, Faculty of Engineering, Shoubra, Benha University, Cairo, Egypt, Email: andrew.bekhit@feng.bu.edu.eg*

2 Experimental Programs

2.1 Specimens' Geometry and Dimensions

A CFS Zee section (200Z20) was used in the study. The 200Z20 had a total web depth of 200 mm, and a flange width of 60 mm with a lip length of 20mm at 45 degrees with a constant nominal sheet thickness of 2 mm as shown in Fig. 1. The CFS-Zee section is mainly controlled by local buckling on the web, so a notch was added to the web, as shown in Fig. 1, to prevent the performance of web local buckling. Specimens' lengths (L) were chosen to isolate each buckling limit state. Their predicted compression capacities were governed by either local, distortion, or global buckling as predicted by the American Iron and Steel Institute (AISI) [22] using the DSM. Specimens with 600mm length and no wed notch were used for local buckling investigations, while specimens with 1000mm and 2500 lengths and with web notch were used for distortion and local buckling investigations, respectively. The finite strip eigen-buckling analysis software CUFSM [23] was used to calculate the elastic buckling loads for local buckling, Pcrl, distortion buckling, Pcrd, and the global buckling, Pcre, and the associated buckling half-wavelengths (Lcre, Lcrd, and Lcrl) respectively.

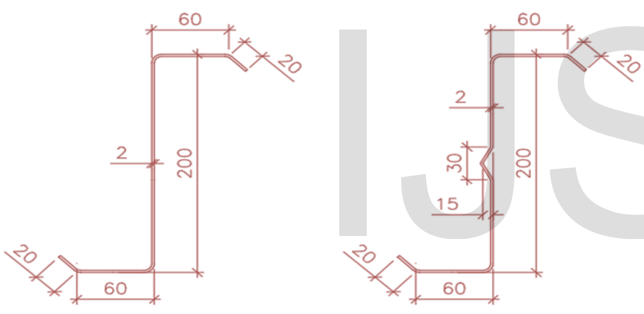

Fig. 1. Zee section - Zamil profile without notch.

2.2 Material properties:

The material assessment of the steel used in the experiments was carried out by performing coupon tests on five randomly selected samples, as shown in Fig. 2. Tests were performed using a GALBADINI test machine with a maximum tension capacity of 10 tons. The coupon tests were performed according to ASTM E8M-16. The tensile coupons were positioned in the machine with friction grips and were ensured that each specimen was aligned vertically and horizontally between the grips. The tensile yield stress was determined from the coupon test for the CFS zee sections was 420Mpa.

2.3 Specimens' imperfection

Defects and imperfections in the CFS thin-walled sections can be classified into material defects and geometric imperfections. This imperfection of the materials includes variation from nominal in elastic modulus, E, yield stress, Fy, and residual stresses or strains. The geometric imperfections include cross-section imperfection, out-of-straightness, inaccurate element dimensions, or general shape irregularity. Those may form during shipping, storage, and machining. The imperfections and the out-to-out dimensions of the flange, web, and lip are considered by using calipers and reference laser tools plates for an average of three locations on specimens; at mid-length, top, and bottom that are summarized in Table 1.

Fig. 2. Tensile Testing Machine

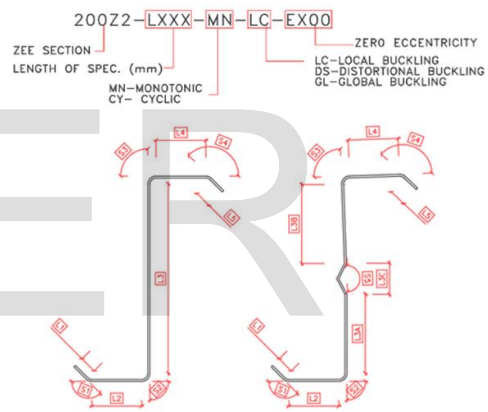

Fig. 3. Strategies for specimens named and imperfection

2.4 Test setup and instrumentation

A dynamic actuator DTE model (LPA-SS-10) having a maximum stroke of 254mm and max a force of 245 kN with a working pressure of 20.7 bar was used in the test's conduction. The actuator was assembled to perform the cyclic tests, as shown in Fig. 4. The specimens were welded from both ends with endplates to transfer axial forces while providing rotation fixed conditions, as shown in Fig. 5.

Table 1 Summary of measured cross-section dimensions

Specimen	S1	S2	S3	S4	S5	L1	L2	L3A	L3B	L3C	L4
	Degree (°)					mm.					
L600CYLCEX00	129	96	92	129	--	18	55	187	51	15	
L1000CYDSEX00	130	89	93	143	181	18	56	70	32	70	60
L2500CYGLEX00	150	92	92	135	180	17	55	72	35	70	54

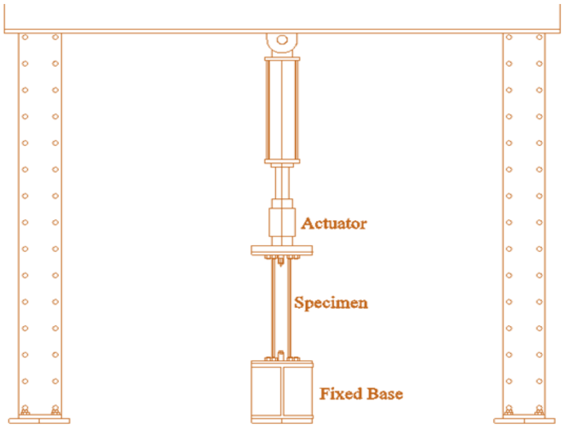

Fig. 4. Specimen Setup.

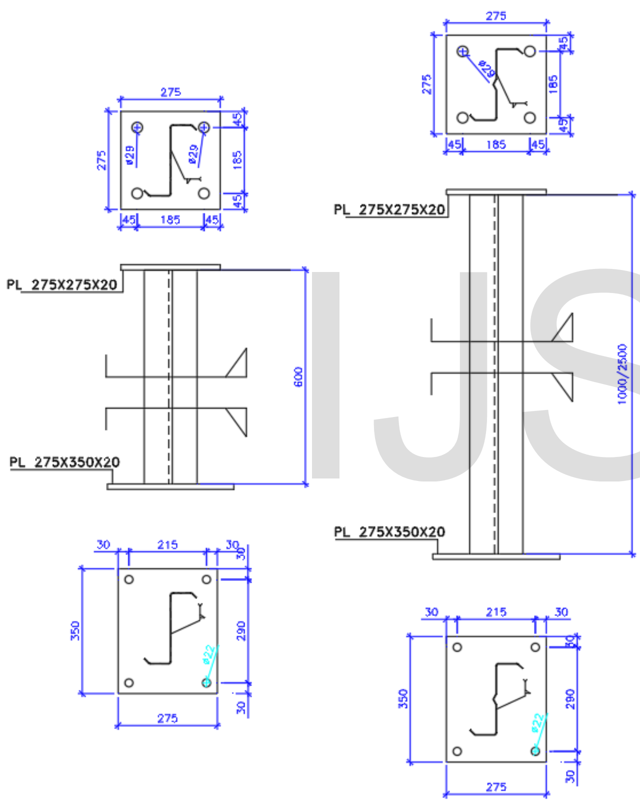

Fig. 5. Endplate fixation for (a) local buckling (b) distortion and Global buckling specimens

Table 2 LVDT location at Specimens

Specimen	Lc	Ld	Lb	Le
	mm	mm	mm	mm
L600CYLCEX00	300	300	300	300
L1000CYDSEX00	200	200	100	500
L2500CYGLEX00	1250	1250	1250	1250

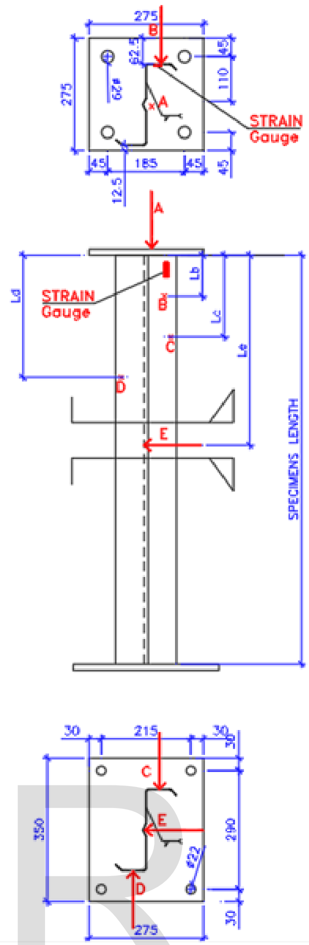

Fig. 6. LVDT locations.

Specimen element deviations were measured using five LVDTs linked to a computer to plot the displacements at their location. The LVDTs are assigned along the length of the specimens, as shown in Fig. 6, and their locations are summarized in Table 2.

2.4 Loading Protocol

The specimens were subjected to quasi-static cyclic displacement history with a constant displacement rate of 0.01mm/sec, which was described by FEMA 461. The deformation-controlled protocol is adopted with FEMA461 quasi-static cyclic protocol, as shown in Fig. 7. In addition, the FEMA 461 protocol was used to capture data on the failure shape, fracture, distortion, and hysterical deformation response characteristics for the elements imposed by the deformations [16]. Moreover, FEMA 461 adapted an asymmetric loading protocol with equal tension and compression displacement. By cycling and repeating the load direction, fracture and tearing occurred, and the load-displacement behavior was thoroughly investigated. In each step in the displacement protocol, the amplitude is increased to its double value per two cycles. Then in the fourth step at the 7th and 8th cycles, the displacement increased to reach the elastic axial displacement δe= PeL/AE. The Pe is the compressive strength calculated by limit states by AISI-S100-16 using the DSM at which buckling deformation occurred. After reaching the fourth step, the amplitude was increased by 40% from the previous strep (i.e., δi = 1.4δi-1).

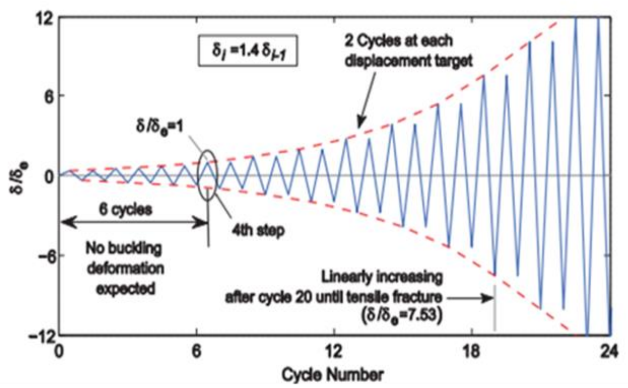

Fig. 7. Cyclic compression-tension loading protocol [10].

Therefore, the protocol of FEMA 461 is defined to allow the member to reach the most severe damage state at the present point in the loading protocol, in the 20th cycle. Also, it is recommended that the lowest fracture and damage states, at least six cycles, be complete [16]. Linear behavior was expected to be achieved for the first eight cycles. In thin-walled CFS, the lowest damage states are considered when the member stiffness degraded due to buckling deformation.

3 Experimental Results

The cyclic response of axial load-displacement (P-δ) for each model, were evaluated. The strength, stiffness, and hysteretic energy dissipated responses were all measured. The cyclic load-deformation responses illustrated individually the local,

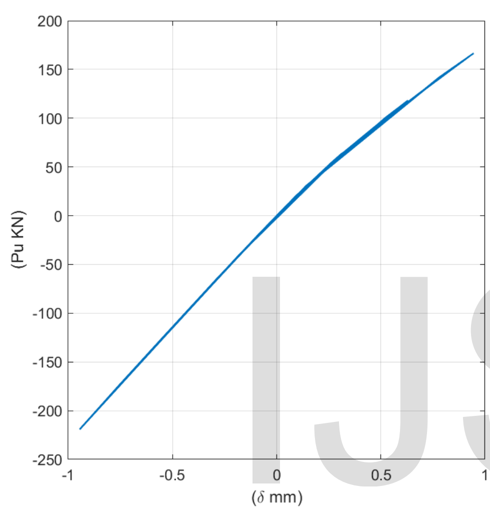

a)

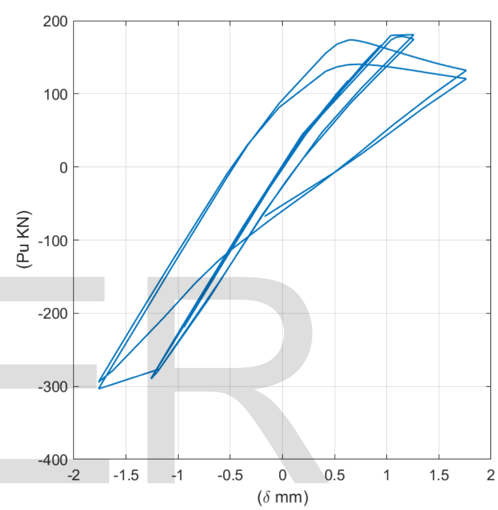

b)

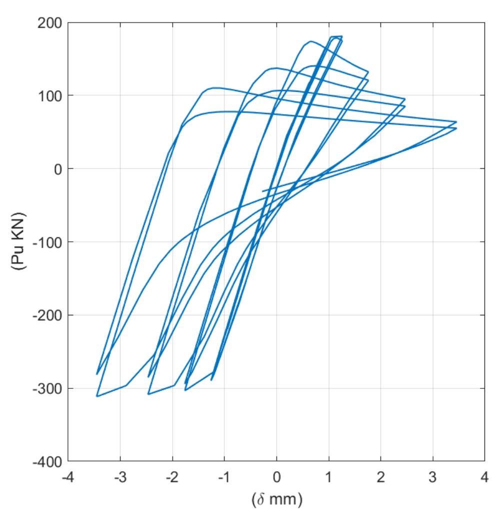

c)

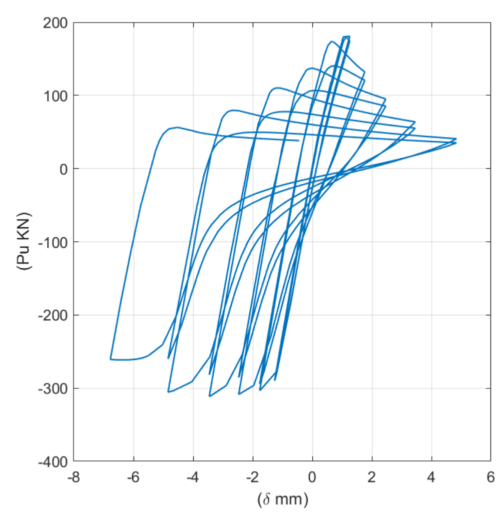

d)

Fig. 9. Cyclic response for L600FL60LIP20 for 6, 12,16, and 20 cyclic of loading

distortion, and global buckling behavior for the zee-section. The CFS zee sections had a linear elastic response for the first six cyclic in the loading protocol, with constant stiffness in the compression and tension zones without inelastic deformation as shown in Fig. 9a. When the applied protocol exceeds the yielding displacement, after 12 and 16 cyclic loadings, a significant permanent deformation occurred and appeared visually. The capacity of the specimens started to decrease rapidly to lose about 60% of the ultimate capacity when reaching the 16 cyclic loading as shown in Fig. 9b and Fig. 9c.

On the opposite side of loading (Tension), the CFS Zee-section can sustain the increase of loads until reaching the peak tension load. So, the cyclic responses had no symmetric peak capacity in compression and tension. Furthermore, strength and stiffness degradation occurred when subjected to repeated compression loads.

For the case of local buckling specimens with a length of 600 mm, the web local buckling and deformation tend to flange as shown in Fig. 10a, which occurred in the lower part of the specimen. The flange and lips are folded outside forming one distortion wave at mid-length of specimen opposite to local buckling failure location. Fig. 10d represented the deformation shape from FE models with the maximum stressed location found near the base.

For the case of distortion buckling specimens with a length of 1000 mm, the flange with lip had at least two half wave lengths along of the specimens' length as shown in Fig. 10 b and Fig. 10 e. The web notch prevents the formation of local buckling in the web, and the distortion buckling is governed. The plastic deformation was formed before the specimens reach their maximum capacity, followed by a post-buckling behavior, and concentrated at corners between web and flanges. The stress in compression and stiffness degraded from inelastic strains showed accumulated damage half-wave the cyclic curve The peak tension strength remained constant until fracture or tearing started at the rounded corners and propagated along with the specimen. For the case of global buckling specimens with a length of 2500 mm, the specimens exhibit global flexure torsion buckling of one half-wavelength at the mid-length of the specimens as shown in Fig. 10 c and Fig. 10 f. The global buckling is associated with the distortion curvature of the flange and tearing in the lip at mid-height.

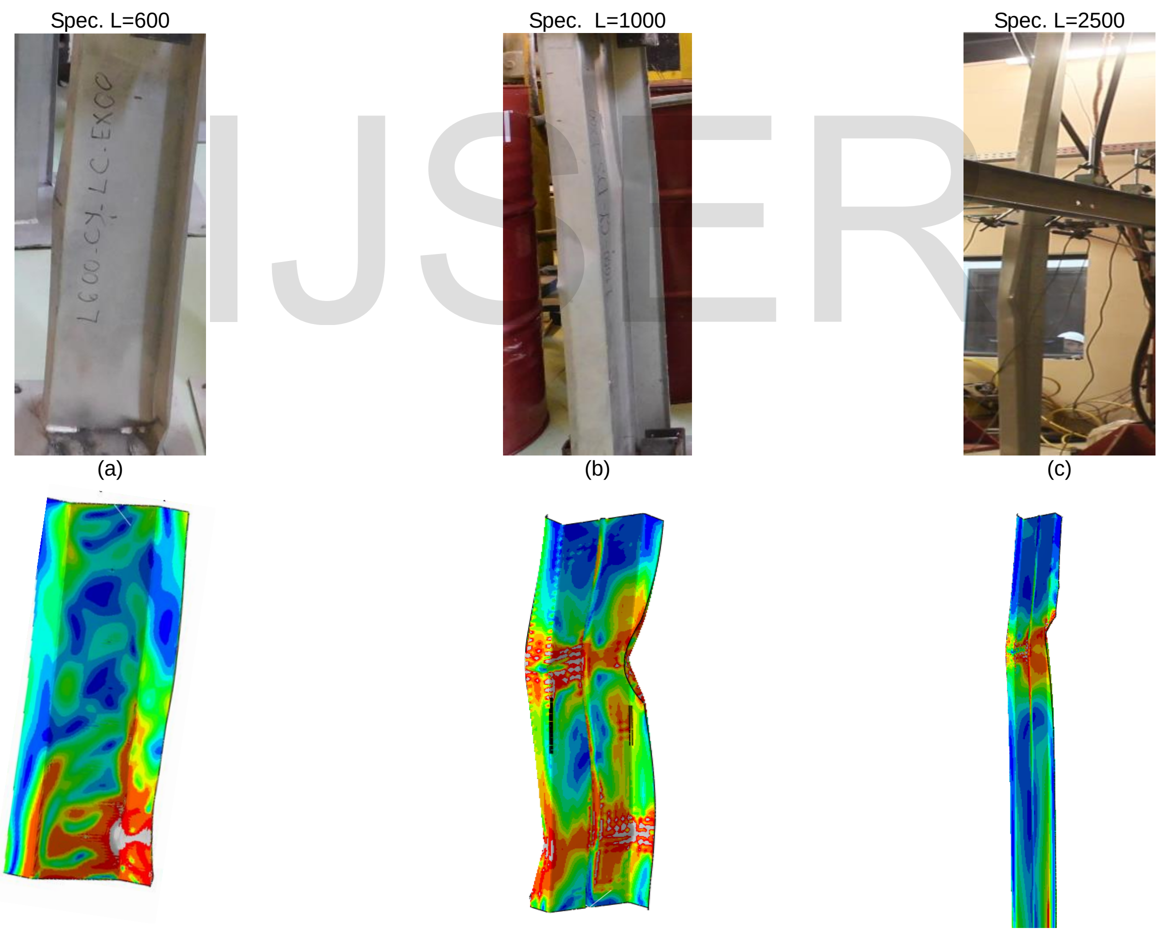

(d) Local buckling in a corner between the web and the flange, as well as the start of flange distortion

(e) Flange distortion, with a folded-out lip

(f) Flange distortion coupled with global buckling

Fig. 10 Verification of Buckling Mode of Experimental against Finite Elements Models

The strength and stiffness are decreased faster when reaching the peak capacity compared with local and distortion specimens. The global specimens lost around 70% of their ultimate capacity strength upon reaching the peak capacity.

3 Verifications:

A FEM for the CFS zee section was performed by ABAQUS soft package. The FEM was based on plasticity using Von misses yield surface and combined hardening parameters assigned to material behavior. Also, material damage and its propagation were assigned in ABAQUS using the ductility damage and damage evolution commands.

The FEM peak capacity in tension and compression results were compared with the experimental results for verification as shown in Table 3. The Means and Coefficient of variation COV for PTest/PFE was equal to 0.98 & 0.031 for tension and 1.03 & 0.05 for compression, respectively. Therefore, it can be concluded that the behavior of CFS was well simulated and representable in the FEM.

4 Parametric Study:

A comprehensive study was performed to create CF-Zee section numerical models subjected to cyclic loading cases. It was generated by adopting a wide range of Zee-section geometry. The flange width (FL) was chosen varied from 60 to 100mm by an increment of 20mm, with changing the lips depth (LIP) by 10, 20, and 30 mm and the thickness (T) by 1, 2, 3, and 4 mm. The element lengths were selected taking into consideration all the buckling failure modes. The elements were selected with L=600mm for the case of local buckling failure, L=1000mm for the distortion buckling failure, and L=2500mm for the global buckling failure. All these investigating models were subjected to concentric cyclic load using FEMA protocol related to each yielding displacement. Yield displacement is estimated based on model dimension and length to assign cyclic load technique. The specimens were labeled to identify the details of FE models; for example, a specimen labeled L1000FL80LIP20-T3EX00 is described as follows: L1000 is the total length of the specimen in mm, FL80 is the flange width in mm, LIP20 is the lip length in mm, T3 is the thickness in mm, and EX00 is the loading eccentricity from the center. The parametric analysis considered the material attributes that are employed in verification models. The experiments used fixed support for both ends as a boundary condition. Load-displacement curves, at the loading point, were extracted and the relationship was simplified, and the S- curve was produced. The peak locations of the member hysteresis curves were evaluated from the S-curve. Under cyclic loading, the members' ultimate capacity would be exceeded by a certain amount of plasticity. Furthermore, when the number of cycles grows, the damage accumulation of the members continued to rise, performing the element deterioration. As a result, the S-curve indicated the cyclic loading induced loss of structural performance and defined the hysteresis features.

The S-curve utilizing FL80, FL100 with Lip depth 20mm and thickness of 3, 4 mm were presented in Figs. 11, 12, and 13, for local, distortion, and global buckling specimens respectively. Also it presents the effect of increasing the thickness of Zee-sections with different flange widths and lip depth. Increasing the thickness of the CFS-Zee section increases the capacity and strength and reduces stiffness degradation after reaching the peak compression strength and increases the tension capacity. Moreover, the effect of lip depth increases with increasing thickness and leads to less energy dissipation. Furthermore, after reaching peak strength, specimens controlled primarily by distortion buckling had a faster decline in stiffness and energy dissipation than those controlled by global buckling. In all cases, the models reached the peak strength then degraded slowly and stabilized around 20% to 30% of their capacity. Lip depth of 10 mm gives more smoothing in the hysterical curve than lip depth of 30mm in local and distortion specimens. Global buckling effect in stiffness and strength degradation may be neglected after reaching peak compression capacity and increasing the thickness from 1 to 4mm increases the section capacity.

Table 3 Experimental and FE results for CFS Zee-section under cyclic load

Specimens' label	$P_{min-Test}$ KN	$\delta_{min-Test}$ mm	P_{min-FE} KN	δ_{min-FE} mm	$P_{max-Test}$ KN	$\delta_{max-Test}$ mm	P_{max-FE} KN	δ_{max-FE} mm	$P_{min-Test}/P_{min-FE}$	$P_{max-Test}/P_{max-FE}$
L600-CY-LC	-179	-2.56	-185.5	-2.52	128.3	1.27	121	1.24	0.96	1.06
L1000-CY-DS	-189.9	-3.2	-186.3	-2.83	113.6	3.01	117.6	2.22	1.02	0.97
L2500-CY-GL	-192.7	-3.88	-200.4	-3.94	82.9	3	78.2	3.05	0.96	1.06
Mean for Specimens									0.98	1.03
The Standard deviation for specimens									0.03	0.052
COV for Specimens									0.04	0.05

$P_{min-test}$, $\delta_{min-test}$ = ultimate capacity in tension and corresponding displacement from experimental.
$P_{max-test}$, $\delta_{max-test}$= ultimate capacity in compression and corresponding displacement from experimental.
P_{min_FE}, δ_{min_FE} = ultimate capacity in tension and corresponding displacement from FE model.
P_{max_FE}, δ_{max_FE}= ultimate capacity in compression and corresponding displacement from FE model.

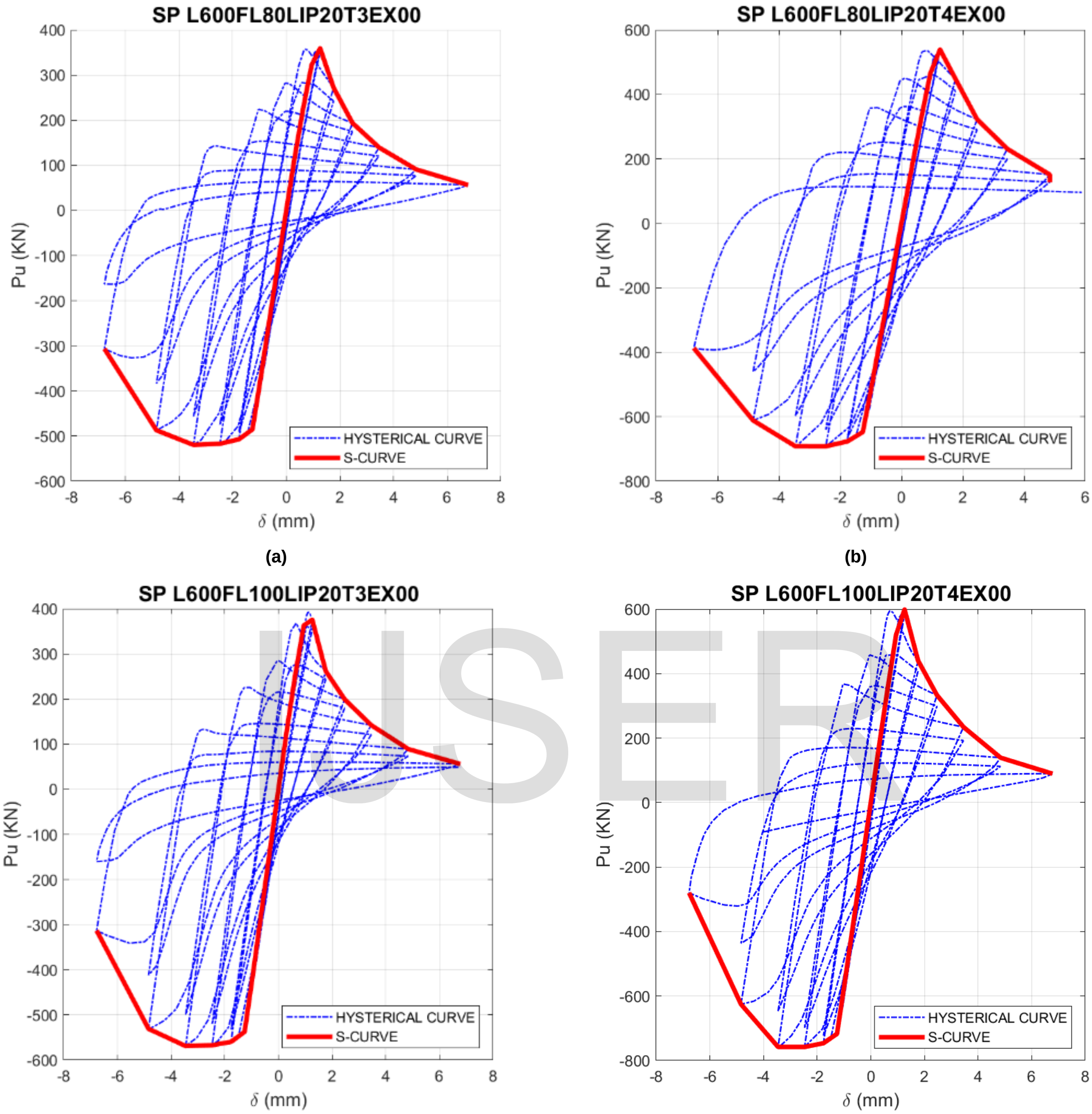

Fig. 11 Hysterical curves with S-curve for Local Buckling Specimens; a) Flange width 80mm and thickness 3mm, b) Flange width 100mm and thickness 4mm, c) Flange width 100mm and thickness 3mm, and d) Flange width 100mm and Thickness 4mm

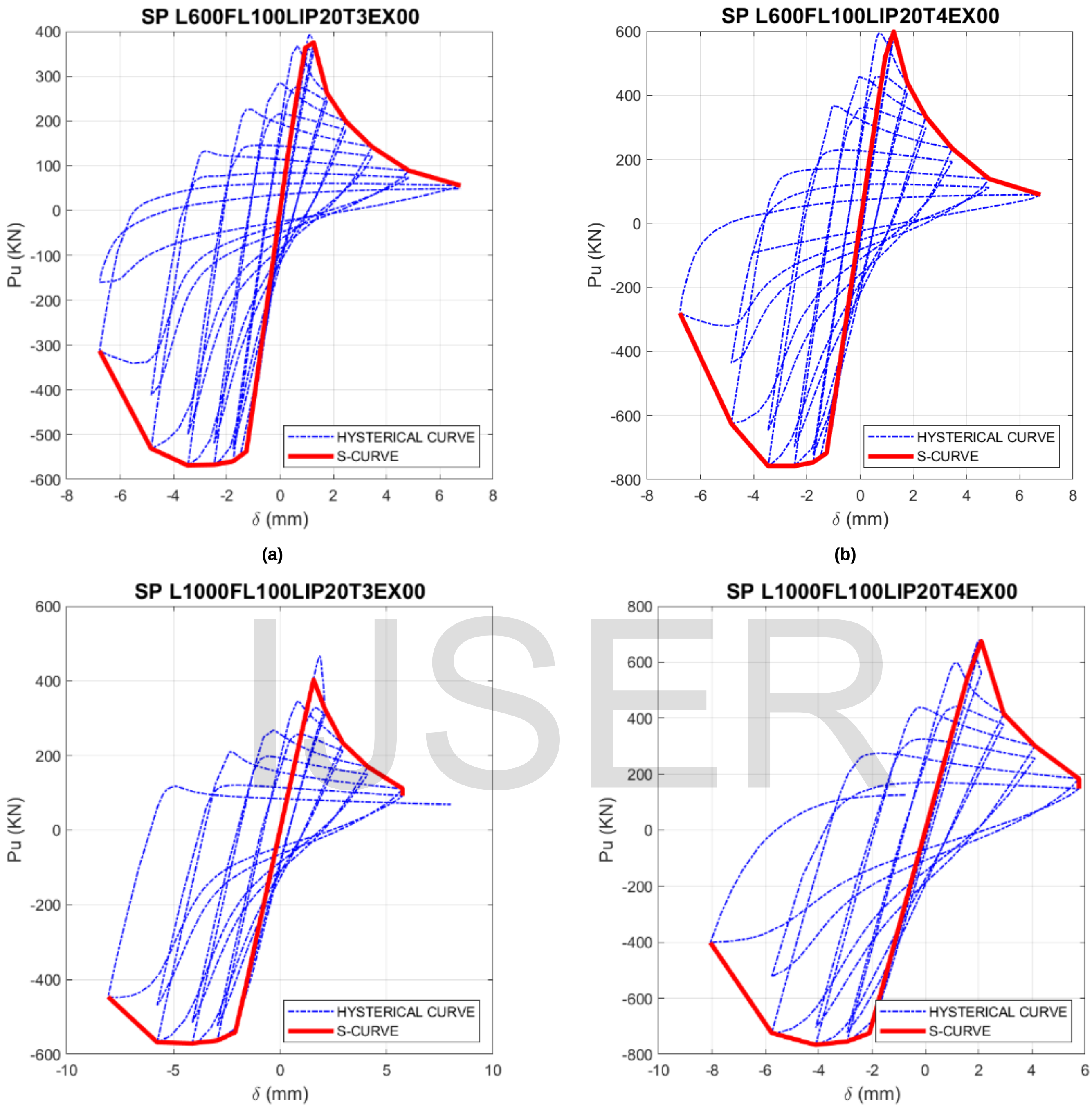

(c) (d)

Fig. 12 Hysterical curves with S-curve for Distortional Buckling Specimens; a) Flange width 80mm and thickness 3mm, b) Flange width 100mm and thickness 4mm, c) Flange width 100mm and thickness 3mm, and d) Flange width 100mm and Thickness 4mm

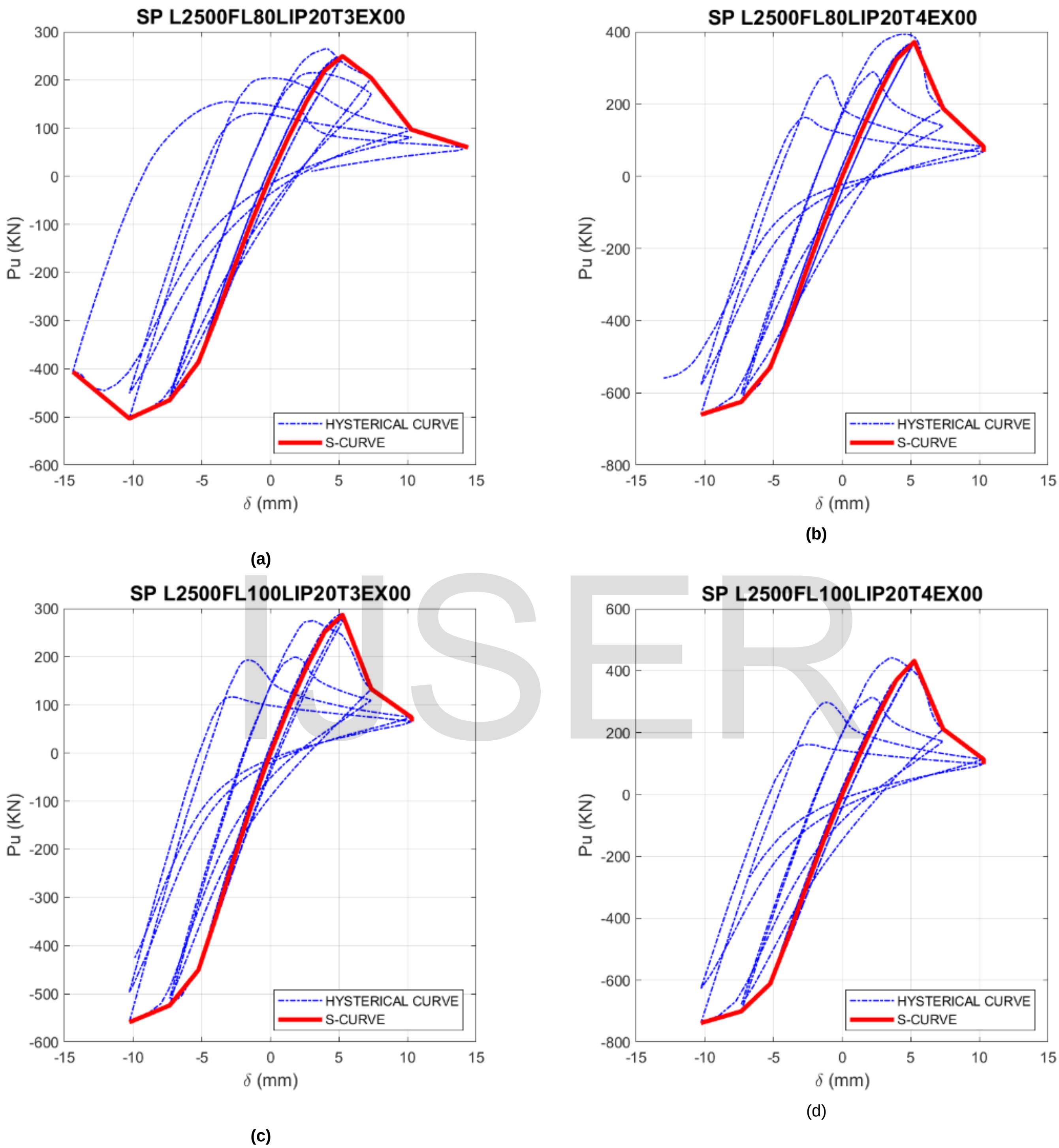

Fig. 13 Hysterical curves with S-curve for Local Buckling Specimens; a) Flange width 80mm and thickness 3mm, b) Flange width 100mm and thickness 4mm, c) Flange width 100mm and thickness 3mm, and d) Flange width 100mm and Thickness 4mm

4 Conclusion

The cyclic response of the CFS-Zee section subjected to local, distortion, and global buckling was investigated.

The load-deformation response and strength deterioration of CFS axial members were evaluated using three full-scale cyclic compression-tension tests. ABAQUS software was used to perform a FEM, which was validated by the experiment results. A parametric study was conducted for CFS–Zee sections with different lip depth, flange width, thickness, and element lengths.

The following are the summary of the findings:

1. In local buckling specimens, the stresses were concentrated at the bottom corner between the web and the flange, and at flange with lip in distortion specimens, and at mid-height for global specimens with flange distortion.
2. In local buckling specimens, the breakdown occurred near the base of the specimens in flange and web, and two waves flange distortion occurred as the specimen as the specimen's length greater than Lcr.
3. In Distortion buckling specimens, the flange distortion was more visible than web local buckling caused by web stiffening, lip floated with a flange along the length of the specimens.
4. Under Cyclic loads, the capacity in compression of the specimens started to decrease rapidly to lose about 80% of the ultimate capacity when reaching the 16 cyclic loadings.
5. In global buckling, specimens lost about 60% to 70% of their potential capacity before achieving peak capacity compared to local and distortion specimens.
6. The CFS-Zee section captured the increase of loads in tension for several cycles until the formation of fracture or tearing.
7. From the parametric study results, the thickness increases the CFS capacity and quick strength and stiffness degradation after reaching the peak compression strength.
8. Decreasing lip depth sustained more capacity in the hysterical curve in local and distortion specimens, while its effect was neglectable in global specimens.

REFERENCES

[1] W. Zhang, X. Xu, Y. Zheng, S. Wang, and Y. Li, "Influencing factors analysis on the shear capacity of cold-formed steel-light frame shear walls." pp. 3588-3604.

[2] F. Derveni, S. Gerasimidis, and K. D. Peterman, "Behavior of cold-formed steel shear walls sheathed with high-capacity sheathing," Engineering Structures, vol. 225, pp. 111280, 2020/12/15/, 2020.

[3] I. Shamim, and C. A. Rogers, "Steel sheathed/CFS framed shear walls under dynamic loading: Numerical modeling and calibration," Thin-Walled Structures, vol. 71, pp. 57-71, 2013/10/01/, 2013.

[4] J. Wang, W. Wang, Y. Xiao, and B. Yu, "Cyclic test and numerical analytical assessment of cold-formed thin-walled steel shear walls using tube truss," Thin-Walled Structures, vol. 134, pp. 442-459, 2019/01/01/, 2019.

[5] D. A. Padilla-Llano, C. D. Moen, and M. R. Eatherton, "Cyclic axial response and energy dissipation of cold-formed steel framing members," Thin-Walled Structures, vol. 78, pp. 95-107, 2014/05/01/, 2014.

[6] A. K. Jain, R. D. Hanson, and S. C. Goel, "Hysteretic Cycles of Axially Loaded Steel Members," vol. 106, no. 8, pp. 1777-1795, 1980.

[7] A. Ucak, and P. J. J. o. S. E. Tsopelas, "Load path effects in circular steel columns under bidirectional lateral cyclic loading," vol. 141, no. 5, pp. 04014133, 2015.

[8] Q. Al-Kaseasbeh, and I. H. J. E. S. Mamaghani, "Buckling strength and ductility evaluation of thin-walled steel stiffened square box columns with uniform and graded thickness under cyclic loading," vol. 186, pp. 498-507, 2019.

[9] Q. Al-Kaseasbeh, and I. H. J. J. o. B. E. Mamaghani, "Buckling strength and ductility evaluation of thin-walled steel tubular columns with uniform and graded thickness under cyclic loading," vol. 24, no. 1, pp. 04018105, 2019.

[10] [D. A. Padilla-Llano, "A framework for cyclic simulation of thin-walled cold-formed steel members in structural systems," Virginia Polytechnic Institute and State University, 2015.

[11] D. A. Padilla-Llano, C. D. Moen, and M. R. J. T.-w. s. Eatherton, "Cyclic axial response and energy dissipation of cold-formed steel framing members," vol. 78, pp. 95-107, 2014.

[12] D. A. Padilla-Llano, M. R. Eatherton, and C. D. J. T.-W. S. Moen, "Cyclic flexural response and energy dissipation of cold-formed steel framing members," vol. 98, pp. 518-532, 2016.

[13] F. J. R. C. FEMA, CA, "461-Interim protocols for determining seismic performance characteristics of structural and nonstructural components through laboratory testing, Federal Emergency Management Agency (FEMA), Document No," 2007.

[14] H. Moghimi, and H. R. Ronagh, "Performance of light-gauge cold-formed steel strap-braced stud walls subjected to cyclic loading," Engineering Structures, vol. 31, no. 1, pp. 69-83, 2009/01/01/, 2009.

[15] Z. Chen, S. Yang, and H. Liu, "Research on the constitutive model of cold-formed thick-walled steel under cyclic loading," Journal of Constructional Steel Research, vol. 160, pp. 457-475, 2019/09/01/, 2019.

[16] D. Dubina, "Behavior and performance of cold-formed steel-framed houses under seismic action," Journal of Constructional Steel Research, vol. 64, no. 7, pp. 896-913, 2008/07/01/, 2008.

[17] S. M. Mojtabaei, M. Z. Kabir, I. Hajirasouliha, and M. Kargar, "Analytical and experimental study on the seismic performance of cold-formed steel frames," Journal of Constructional Steel Research, vol. 143, pp. 18-31, 2018/04/01/, 2018.

[18] Y. Hu, L. Jiang, J. Ye, X. Zhang, and L. Jiang, "Seismic responses and damage assessment of a mid-rise cold-formed steel building under far-fault and near-fault ground motions," Thin-Walled Structures, vol. 163, pp. 107690, 2021/06/01/, 2021.

[19] D. P. McCrum, J. Simon, M. Grimes, B. M. Broderick, J. B. P. Lim, and A. M. Wrzesien, "Experimental cyclic performance of cold-formed steel bolted moment resisting frames," Engineering Structures, vol. 181, pp. 1-14, 2019/02/15/, 2019.

[20] J. M. Goggins, B. M. Broderick, A. Y. Elghazouli, and A. S. Lucas, "Behaviour of tubular steel members under cyclic axial loading," Journal of Constructional Steel Research, vol. 62, no. 1, pp. 121-131, 2006/01/01/, 2006.

[21] B. W. J. J. o. c. s. r. Schafer, "The direct strength method of cold-formed steel member design," vol. 64, no. 7-8, pp. 766-778, 2008.

[22] A. Iron and S. Institute, "AISI-S100-16: North American specification for the design of cold-formed steel structural members," ed: ANSI/AISI Washington, DC, 2016

[23] B. J. D. o. C. E. Schafer, http~//www, ce. jhu. edu/bschafer/cufsm/, . Johns Hopkins University, "CUFSM 5.01—Elastic Buckling Analysis of Thin-walled Members by the Finite Strip Method and Constrained Finite Strip Method for General End Boundary Conditions. Department of Civil Engineering, Johns Hopkins University," 2012J.S. Bridle, "Probabilistic Interpretation of Feedforward Classification Network Outputs, with Relationships to Statistical Pattern Recognition," *Neurocomputing—Algorithms, Architectures and Applications,* F. Fogelman-Soulie and J. Herault, eds., NATO ASI Series F68, Berlin: Springer-Verlag, pp. 227-236, 1989. (Book style with paper title and editor)